JOURNAL OF MATERIALS SCIENCE 26 (1991) 6423–6430

Investigation of the adhesion toughness of lacquer to zinc-phosphated steel

Y. M. ARAVOT, A. ALBU-YARON*
ARO, The Volcani Center, PO Box 6, Bet Dagan 50250, Israel

A shear test under uniform plane stress loading conditions at the interface has been used to evaluate the adhesion toughness of the bond of a fast-cure thermosetting powder coating to zinc-phosphated cold-rolled steel surfaces of two different origins. The shear test is designed to measure the nominal and the net ultimate shear stress (USS) values, as well as the critical stress intensity factor of interfaces. The experimentally measured critical load at which the adhesion failed, together with the ultimate shear stress values calculated and fractographic analysis of shear-failed specimens on mating surfaces, were used to quantify the bond toughness along the interfaces of zinc-phosphated cold-rolled steel–lacquer specimens, and to provide an insight into fracture phenomena and adhesion mechanisms. It was shown that differences between these two layers manifested by change in the USS net value are due to variation in the morphology of the two zinc phosphate conversion layers studied.

1. Introduction

The adhesion of polymeric materials to metallic substrates is important in many approaches of science and technology but without doubt the area which has received most attention is corrosion protection [1–3]. The toughness of the adhesive bonding at the metal–organic coating interface level has generated a fair number of recent reviews [4–6]. It has been demonstrated that the single most important step in the adhesive process is the surface pretreatment of the metal substrate, as it has a direct impact on the performance of the bonded structure.

In the case of cold-rolled steel (CRS), surface pretreatments generally involve a phosphating step forming an inorganic insulating phosphate layer of manganese, iron, zinc or calcium phosphate [7–9]. These conversion layers, which produce compositional, mechanical and microstructural changes in the surface and near-surface region of the material, impart, besides better lacquer adhesion, a new physical and physicochemical character to the CRS surfaces, such as lacquer wettability, good mechanical characteristics and improved corrosion resistance.

As far as corrosion of the metallic substrate is concerned – paint delamination on cold-rolled steel is reported to occur by the shear action of corrosion products – the insertion of phosphate conversion layers improves the adhesion toughness by inducing toughening processes. For these toughening mechanisms to occur, the interface between the lacquer and the conversion coating material must be strong in shear so that the lacquer layer cannot debond from the metal base material at a suitable level of applied stresses (like corrosion products, etc.).

Little is known, however, about how to optimize the structure and morphology of conversion layers and interfaces in these materials to achieve high values of adhesion toughness, even though the importance of being able to "tailor" the interface to achieve desirable adhesion and mechanical properties is now widely recognized.

In a previous study of iron phosphate pretreatment effects on CRS, we attempted for the first time to determine the shear strength of lacquer–iron-phosphated CRS interfaces in an effort to obtain quantitative information about the weak boundary in these systems [10, 11]. We used the modified Arcan *et al.* [12] method for testing material properties under uniform stress-state fields to quantify the toughness of bonding of a fast-cure thermosetting powder coating to an iron-phosphated CRS and a control non-treated CRS surface. The test considers adhesive failure a fracture process and uses the shear stress value at failure as the quantitative information of the bond toughness along the interface. Results from previous work have shown that ultimate shear stress values (USS_{net}), calculated from the experimentally measured critical load at which the adhesion failed, reveal variables influencing adhesion such as type of CRS, pretreatment or variations in stoving temperatures. We describe here the assessment of the method to quantify the relative toughness of the bond of a fast-cure thermosetting powder coating (L) to cold-rolled steel–zinc phosphate surface treated in two different industrial processes (PZn1 and PZn2), and to compare the results with a control, unmodified steel surface, and with an iron phosphate-pretreated surface.

* To whom all correspondence should be addressed.

0022–2461/91 $03.00 + .12

2. Materials

Standard cold-rolled steel panels, ~ 1.25 mm thick, manufactured by two suppliers (S3 and S4) were used as metallic substrate material. Zinc phosphating on both the steel sheets was performed in two different industrial plants under controlled conditions following coating procedures recommended by the manufacturer's specifications (S3PZn1, S3PZn2, S4PZn1, S4PZn2). The resulting zinc phosphate thicknesses, determined by chemical stripping, indicated that the coating weights in all cases were typically ~ 2.3–2.7 μm (2.0–2.4 g m^{-2}). Additional iron-phosphated cold-rolled steel specimens (S3P, S4P) on the same steel substrates (S3 and S4), obtained from the plant production line of Pachmas, were about 0.4 μm (0.35 g m^{-2}).

Coating of sheets with a fast-cure (thermosetting epoxy resin/phenolic hardener) powder was carried out on a laboratory scale; the details have been described elsewhere [11].

3. Experimental procedure

3.1. The specimen and mechanics of the test

Specially designed symmetrical test specimens which enable proper mechanical behaviour under shear (initiation of fracture produced intentionally and in a controlled way by two symmetric Teflon strips), and uniform shear stress loading (in the interface plane) throughout direct bonding by crosslinking, were used in this work. The specimen and the testing system were developed to model the complex fracture of the interfaces in these types of material. The geometry of the crosslinked specimen, and the mounting for testing used throughout this work, together with a thorough discussion of the device and mechanics have been presented in previous papers [10, 11].

3.2. Ultimate shear stress determination

Specimens were tested to fracture and the critical load was recorded on an x–y recorder. Load was applied with an Instron (Model 1251) testing system at a crosshead speed of 0.01 mm min^{-1}. A configuration of 30% (initial crack length $a = 12$ mm) symmetrically cracked specimen allowed an area of $A_{net} = 240$ mm^2 out of a section of total nominal area $A_n = bc = 722$ mm^2 coating to be tested [11]. From the experimentally measured critical load at which the interface failed (P_c), the adhesion toughness, usually characterized by the net ultimate shear stress value, $(USS)_{net}$ N mm^{-2} ($\tau_{net} = P_c/A_{net}$), as well as the critical stress intensity factor (SIF) at fracture (Mode II [13, 14]: $K_{IIC} = f_{II}\,\tau_{net}\,[h/(1-\nu)]^{1/2}$, where the correction factor $f_{II} = 1.35$ experimentally determined for stiff adherent specimen and 30% symmetric crack length; h, the lacquer thickness = 0.07 mm; ν, the Poisson coefficient = 0.34) were easily evaluated.

3.3. Fracture surface characterization

Scanning electron microscopy (SEM) and energy-dispersive X-ray analysis (EDS) were carried out simultaneously on the two mating parts of the freshly fractured specimens following the shear fracture test, to determine the adhesion failure mode and the locus of failure at the interface, as well as to explain differences in USS_{net} values. A Jeol JSM-T330A SEM, fitted with a Proxan III energy-dispersive X-ray spectrometer system and interfaced to a PC-XT computer, was used.

Elemental compositional analysis was carried out on both sides of the fracture, at several locations of the fracture sampled area. Typical X-ray spectra were obtained using 10–20 kV electrons and a specimen current of 5–20 nA.

4. Results

4.1. Shear test results

To evaluate the adhesion toughness at interfaces in the case of adhesive bonding of a fast-cure thermosetting powder coating (L) and zinc phosphate pretreated cold-rolled steel (SPZn): SPZn-L, shear tests were conducted and results for USS_{net} values compared with those of adhesion forces of two different substrates: an iron phosphate pretreated steel substrate (SP) and a control unmodified steel (S) substrate surface. The results of the tests are presented in Table I (USS_{net} and K_{IIC}) and in Figs 1a, b and 2 (USS_{net} only). Each data point represents the mean value and standard deviation of a minimum of 12 test specimens.

Figs 1a and b present variations of USS_{net} values versus treatment at two stoving temperatures and for two zinc phosphating conditions in the case of cold-rolled steel of two different provenances S3 and S4, respectively. The inset shows the configuration – pure sheer mode – of the test fixture and loading system. Shear strength values of 30–40 N mm^{-2} were obtained for the S3 and S4 specimens which were not zinc-phosphate pretreated before coating (control).

TABLE I Basic mode II mechanical properties of lacquer–steel specimens

Specimen	USS_{net} (N mm^{-2})	K_{IIC} (N mm$^{-3/2}$)
S3PZn1L200	42.6 ± 2.6	18.4
S4PZn1L200	41.9 ± 2.5	18.0
S3PZn2L200	16.0 ± 2.5	6.9
S4PZn2L200	20.2 ± 5.0	8.7
S3PZn1L220	42.7 ± 3.0	18.3
S4PZn1L220	43.3 ± 3.1	18.6
S3PZn2L220	11.3 ± 0.7	4.8
S4PZn2L220	17.0 ± 1.8	7.3
S3PL200	44.8 ± 0.6[a]	19.4
S4PL200	43.3 ± 2.6	18.6
S3PL220	46.8 ± 0.2[a]	20.2
S4PL220	45.1 ± 2.5	19.4
S3L200	36.2 ± 1.8[a]	15.5
S4L200	33.7 ± 2.9	14.5
S3L220	40.7 ± 2.5[a]	17.5
S4L220	37.8 ± 3.0	16.2

[a] From Aravot *et al.* [11].

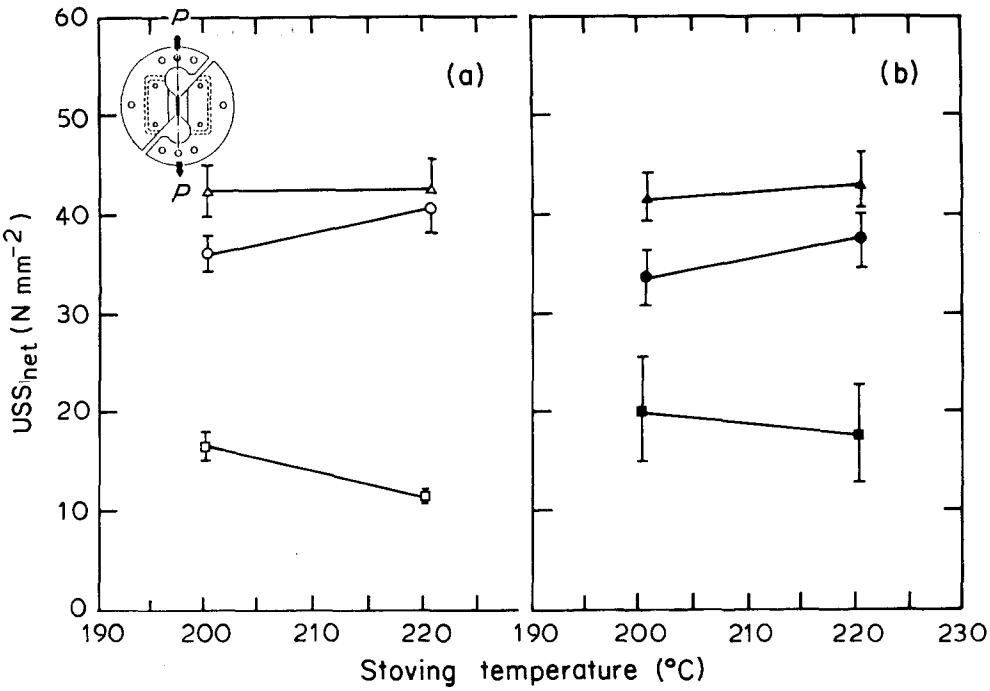

Figure 1 Adhesion characteristics: effect of zinc phosphate treatment on USS_{net} values in the shear test. (a) S3 substratum: (○) S3L, (△) S3PZn1L, (□) S3PZn2L; (b) S4 substratum: (●) S4L, (▲) S4PZn1L, (■) S4PZn2L. Inset: the circular test frame for pure shear mode loading.

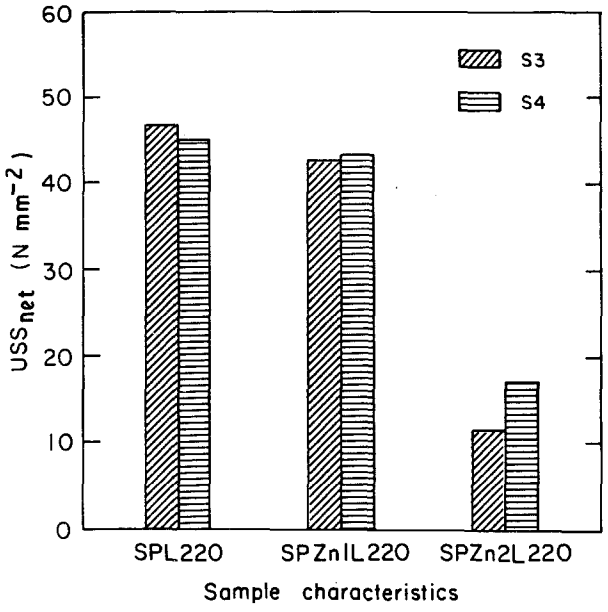

Figure 2 Adhesion characteristics: effect of type of conversion layer formed on cold-rolled steel substrata S3 and S4 on USS_{net} values in the shear test.

Specimens given a zinc phosphate pretreatment exhibited shear strength values ranging from 11–20 N mm^{-2} for zinc phosphate pretreatment 2 (PZn2) to 42–44 N mm^{-2} for zinc phosphate pretreatment 1 (PZn1). These figures indicate that zinc phosphate pretreatment of steel promotes, in the case of PZn1, higher USS_{net} values, suggesting good adhesion. In the case of PZn2 pretreatment, considerably lower USS_{net} values developed (lower than at control, non-pretreated steel–lacquer interface system). We believe this deviation from the normal 40 N mm^{-2} behaviour of conversion coatings on steel to be due to some material peculiarities.

The effect of lacquer stoving temperature on the initial adhesion strength of lacquer–zinc-phosphated and zinc-phosphate-free cold-rolled steel interfaces is also shown in Fig. 1a and b for S3 and S4-type cold-rolled steel, respectively. Two different trends were observed: (i) systems developing high USS_{net} values (> 40 N mm^{-2}) at interfaces (zinc phosphate pretreatment 1: S3PZn1L, S4PZn1L) for which an increase in stoving temperature (200–220 °C) promoted a moderate increase in USS_{net} values; and (ii) systems exhibiting considerably lower USS_{net} values (15–20 N mm^{-2}) (zinc phosphate pretreatment 2: S3PZn2L, S4PZn2L) for which the increase in stoving temperature developed a significant decrease in USS_{net} values (15–25%).

A comparison of the initial adhesion strength of the same lacquer (L) to different conversion layers formed on S4 cold-rolled steel base material – an iron phosphate and two different zinc phosphate layers – is presented in Fig. 2. Results from shear failure tests at a lacquer stoving temperature of 220 °C showed superior bond forces ($USS_{net} > 42$ N mm^{-2}) for the iron phosphate pretreatment and the zinc phosphate pretreatment 1 systems, two to three times higher than that measured in the case of the zinc phosphate pretreatment 2 system ($USS_{net} \sim 18$ N mm^{-2}).

4.2. SEM of as-deposited zinc phosphate layers on CRS

SEM analysis of the two zinc phosphate conversion layers (PZn1 and PZn2) on cold-rolled steel prior to lacquer coating was attempted in order to understand the film dimensions and morphology.

There are obvious differences between the surface morphologies of PZn1 and PZn2 films as revealed by the photomicrographs in Figs 3 and 4 according to, in particular, the phosphating procedure. Both the micrographs emphasize the two-dimensional (e.g. plate-like) structure of the zinc phosphate particles comprising the films, with striking differences in surface morphologies from being extremely rough in the case of PZn1 to smooth in the case of PZn2 film.

Zinc phosphate deposited by process 1 appears to grow in distinct, large plate-like shaped, interlocking crystals (Fig. 3), having various orientations outwards and laterally over the substrate surface. Their edge lengths measure 5–12 μm and their thickness ~ 0.2 μm. They exhibit good cohesion properties and are adherent to the CRS base material. The surface morphology of zinc phosphate deposited by process 2 has the same large, plate-like shaped crystals but shows, in contrast, a distinct growing habit almost parallel (0–20°) to the steel substrate surface. They exhibit a porous flaky structure, with poor bonding between crystals but adherent to the cold-rolled steel base material. The typical crystal size of PZn2 was larger (10–30 μm) than the average crystal size of PZn1. The layer thickness averages, in all cases, 2.4 μm for both the zinc phosphate conversion layers. Although the coating mass did not depend on the phosphating process of either process 1 or 2, or on CRS base material S3 or S4, the average crystal habit – for instance the surface morphology of films – was closely related to the zinc phosphating procedure.

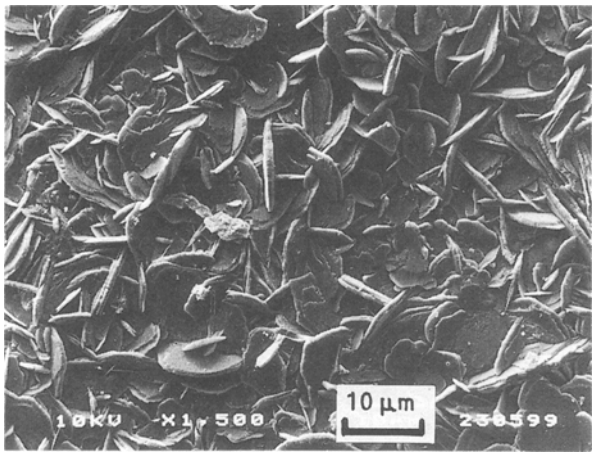

Figure 3 SEM micrograph showing the initial surface morphology of the zinc phosphate layer from process 1 produced on cold-rolled steel substratum S3 or S4.

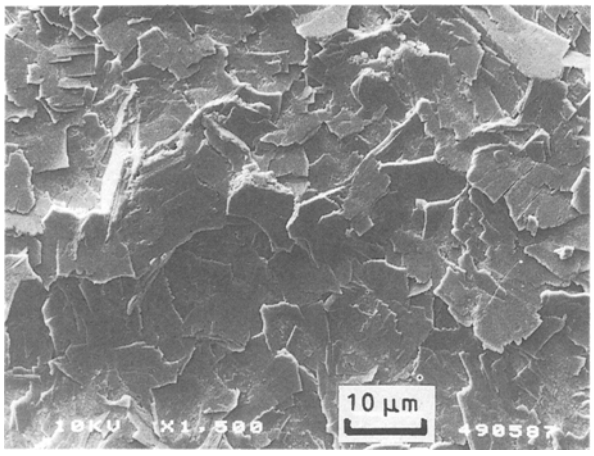

Figure 4 SEM micrograph showing the initial surface morphology of the zinc phosphate layer from process 2 produced on cold-rolled steel substratum S3 or S4.

4.3. Fractography of the shear-tested specimen

We applied SEM and EDS to the study of both sides of the interface fracture in order to explain the variations in adhesion toughness measurements between the two lacquered zinc-phosphated CRS samples differing only in their phosphate substrate properties.

The SEM micrographs in Figs 5 and 6 reveal details of the fracture pattern after shear failure, characteristic of the zinc phosphate pretreatments 1 and 2, respectively. Significant differences could be observed. The micrographs in Fig. 5 show the two mating surfaces (Fig. 5a and b – the lacquer side, and Fig. 5c – the metal side) of the SPZn1L system fracture resulting from the shear test. The fracture surfaces are rough, showing on the metal side (Fig. 5c) interlocked zinc phosphate crystals surrounded by areas of remnants of lacquer whiskers with plastic deformation, while on the lacquer side remnants of zinc phosphate crystals could be observed at higher magnification (Fig. 5a). This observation was also supported by examination of fracture surfaces. Inclusions in the lacquer (arrow in Fig. 5a) were analysed by EDS and constituents from both the metal support (zinc and phosphorus) and lacquer layer (titanium) were detected (Fig. 5d). These observations indicate a strong adhesion at interfaces between PZn1 and the lacquer layer, suggesting that when a crack starts, the fracture propagates, changes direction – entering the lacquer bulk as well as the PZn1 bulk – and entwines the interface at random between the cohesive failure of the lacquer and PZn1 layers.

Details of the fracture resulting from shear failure test in the case of PZn2 pretreatment are shown in Fig. 6. Examination of the fracture surfaces reveals the presence of large, layered zinc phosphate crystals on both the lacquer side (Fig. 6a and b) and the metal side of the fracture (Fig. 6c), with their smooth surface appearance. Easily visible on the metal side (Fig. 6c) are occasional remnants of some lacquer whiskers in between the large zinc phosphate crystals. EDS investigation of fracture surfaces strengthens the SEM results, showing the presence of zinc and phosphorus in the areas with smooth appearance on both the fracture surfaces (Fig. 6d). These results indicate that in this system, after the crack starts, fracture propagates mainly in the zinc phosphate bulk, suggesting weaker cohesive bonds within the zinc phosphate 2 film.

These results correlate well with measurements of USS_{net} values in shear test when higher values ($> 42\ N\,mm^{-2}$) were obtained with the SPZn1L system, while very low USS_{net} values (12–18 $N\,mm^{-2}$)

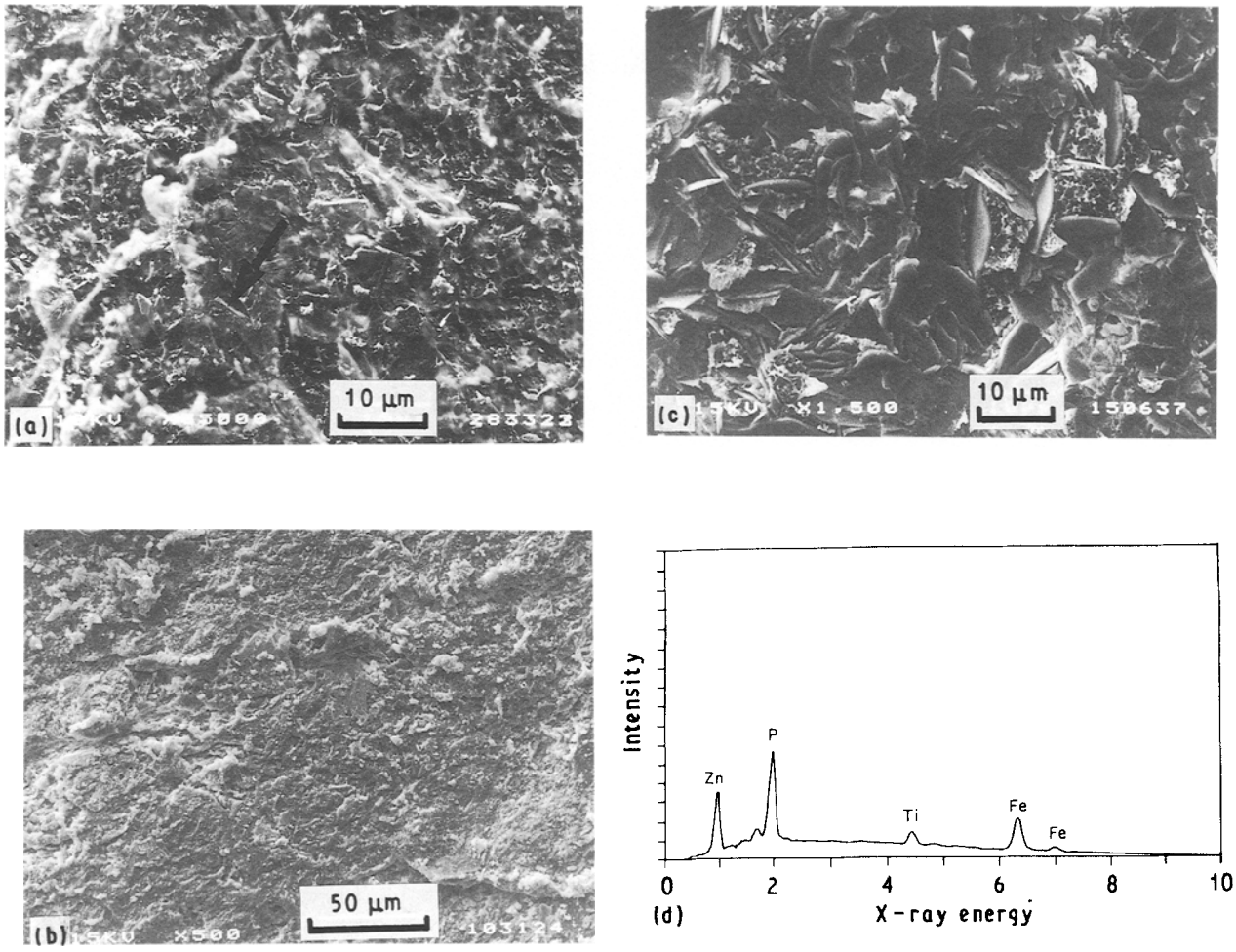

Figure 5 SEM micrographs of typical fracture surfaces of shear-failed SPZn1L specimens: (a, b) lacquer side; (c) metal side; (d) EDS analysis of inclusion from the area marked by an arrow in (a), revealing elements of both the support (peaks of phosphorus and zinc) and lacquer layer (titanium).

were obtained with the SPZn2L system (see also Fig. 1).

5. Discussion

The most striking difference between the two zinc phosphate layers deposited by processes 1 and 2 is the change in USS_{net} values calculated from the experimental measurements described in section 4.1. That this reflects varying bond toughness is seen from results in Table I and Figs 1 and 2.

Phosphating, in general, is used to enhance adhesion between two solid-adhesion partners – e.g. the cold-rolled steel and the organic lacquer in this work – having little bulk chemical affinity. The adhesion force (the force required to separate the two solid partners) is the result of a number of different adhesion-force components of various origin (mechanical; physical – weak van der Waals forces and dipole–dipole interaction; or chemical – strong hydrogen bonding or covalent bonding) acting simultaneously and with a relative involvement depending on the nature of the two solid partners and on the bonding conditions. The resistance of the interface region to the initiation and propagation of fracture depends on the interface chemical bonding (strong forces) and also on the configuration of that interface.

In the case of SL systems, the lack of interface chemical bond suggests that only weak van der Waals physical forces and/or mechanically interlocked structures could contribute to the linkage of these two solids, and this explains the somewhat lower USS_{net} values (30–40 $N\,mm^{-2}$) obtained with these systems.

In the case of SPZnL systems, a most important step in understanding the observed shear strength results and the establishment of the bonds between the two solid-adhesion partners – the zinc-phosphated cold-rolled steel (SPZn1 and SPZn2) mineral-compound substrate and the organic molecules constituting the coating – was to look at the micromorphology and structure of the PZn1 and PZn2 films. The SEM micrographs in Figs 3 and 4 show the remarkable difference in their surface morphology and reveal the strong link in their preparation and existing conditions.

The zinc phosphate structure produced in process 1 with the large, plate-like, chaotic, interlocked crystals, leads to a rough surface morphology as well as improved bulk mechanical properties. We relate the superior adhesion bond ($USS_{net} > 42\,N\,mm^{-2}$), in this case, to bulk-improved stiffness and toughness, and to surface-particle bridging along the interface and plane-toughening effects of the PZn1 structure, together with perhaps the promotion of new interface

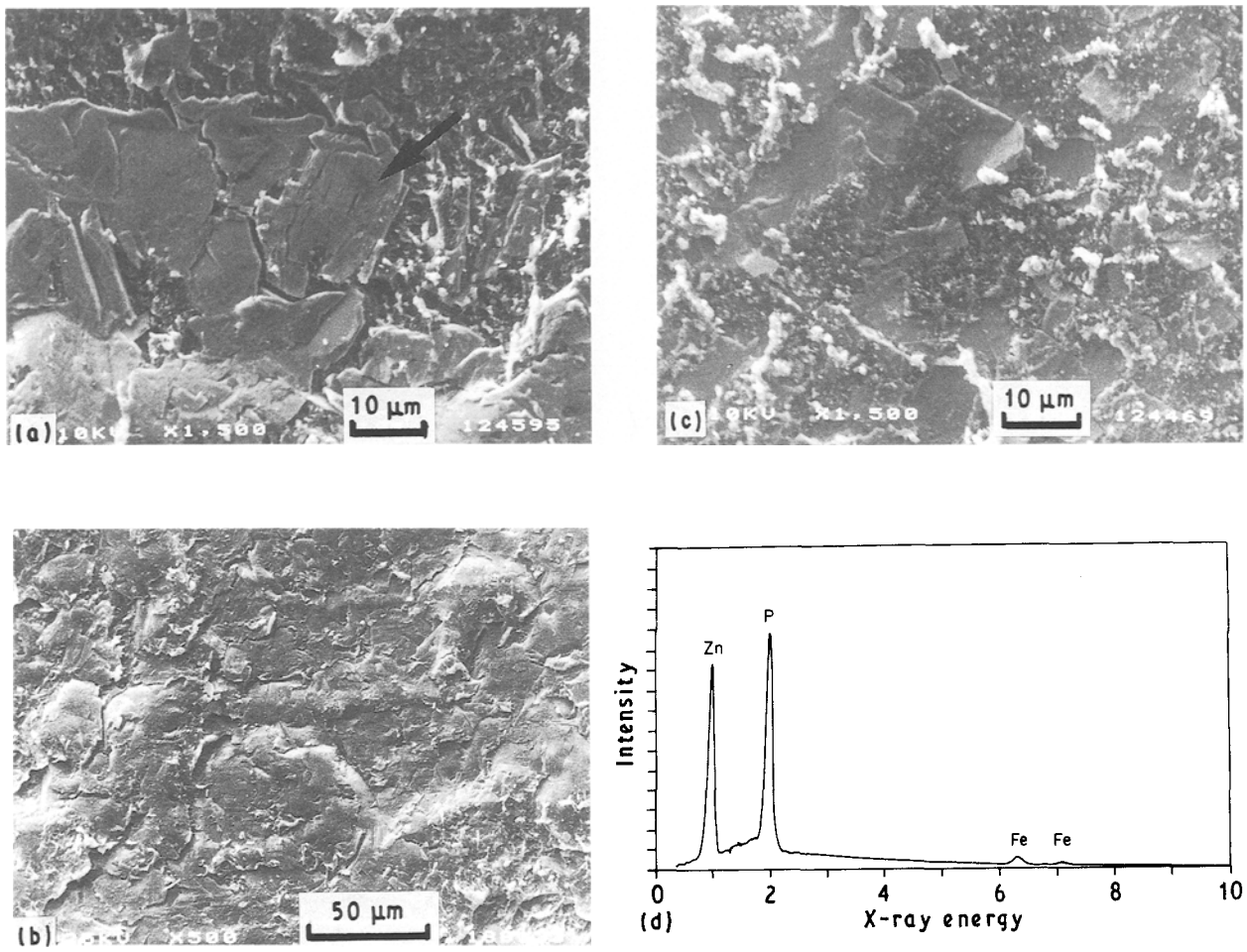

Figure 6 SEM micrographs of typical fracture surfaces of shear-failed SPZn2L specimens: (a, b) lacquer side; (c) metal side; (d) EDS analysis from the area marked by an arrow in (a), revealing zinc phosphate.

chemical bonding created by the phosphating pretreatment. The torturous fracture surface exhibited, on both sides of the fracture after testing, indicating that fracture propagation is more difficult and implying that the direction and magnitude of the local applied stresses are variable, is consistent with the suggested zinc phosphate particle toughening effect along the interface. In this case shear failure propagates mainly at an "interphase"-like region containing the thin lacquer layer and zinc phosphate particles as part of the interface [15]. The high-magnification SEM micrograph in Fig. 7 illustrates conclusively the fibre (polymer) particle (zinc phosphate crystals) – reinforced interface in the SPZn1L system.

This behaviour suggests that in this system the strength of the interfacial bonding in SPZn1-L exceeds the cohesive bonds in both the zinc phosphate and the lacquer layer.

In contrast, the worst-performing zinc phosphate ($USS_{net} < 20\ N\,mm^{-2}$) produced in process 2, with the large plate-like, ordered crystals, parallel to the steel substrate, leads to a relatively flat surface (on a macroscale) and a layered-like structure which excludes perfect cohesion. The smooth appearance of fracture interfaces on mating surfaces, revealing the large zinc phosphate crystals as a homogeneous thin ($\sim 0.20\ \mu m$) film attached to the lacquer (on the lacquer side of the fracture), implies fracture propagation within the phosphate layered structure film.

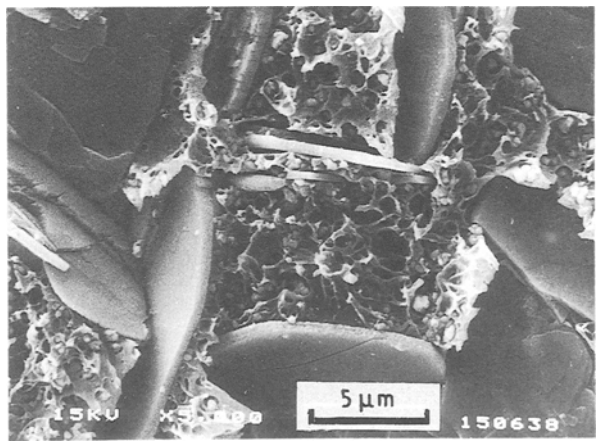

Figure 7 SEM micrograph at higher magnification showing details of the fracture of shear-failed SPZn1L specimen (from Fig. 5a). Note the two solid surfaces being locked via filaments formed by penetration of the organic coating between the PZn1 particles.

We associate the much lower USS_{net} values in the case of SPZn2L systems ($< 20\ N\,mm^{-2}$) with the unusual structure and morphology developed during the phosphating process 2. The layered structure, with zinc phosphate crystals loosely bonded to each other,

favoured easy shear fracture propagation along a plane of least cohesion located within the zinc phosphate 2 film close to the interface proper. The assumption of failure in this plane was supported by EDS investigation of fracture surfaces. Analysis of the large particles visible on the lacquer side of the fracture (Fig. 6a) indicates the presence of substantial amounts of zinc and phosphorus, in addition to components from the lacquer layer (titanium) (Fig. 6d) much larger than those found on the PZn1 fracture, indicating weaker cohesive bonds. In addition, the random remnants of some lacquer whiskers, visible on the metal side of the fracture, imply that only a small amount of polymer in plastic deformation is involved in the fracture, suggesting also weaker bonds.

Since failure was within the zinc phosphate layer in all PZn2 cases and at USS_{net} values much lower than with the control, unmodified steel, it is not known how much the smoother surface morphology or the new chemical bonding simultaneously produced by the phosphating process contributed to adhesion in this case.

We relate the differences in USS_{net} values obtained to the bulk and surface morphology of the two zinc phosphate layers as they form during the phosphating processes 1 and 2. First, the existence of the plane of least cohesion along which failure occurred at much lower USS_{net} values, in the SPZn2L systems, is the result of the boundary existing between lacquer and zinc phosphate crystals at the interface section, together with the cohesive bonds required to obtain perfect cohesion within the bulk material, both operating in the unusual layered-like structure of the zinc phosphate 2 layer. In the SPZn1L systems, the particle toughening effect improved the bulk stiffness and toughness of the zinc phosphate 1 layer. Second, the major topographical differences between the two layers with the formation of a relatively smooth surface (on a macroscale), in the case of zinc phosphate from process 2, explain the small amount of lacquer in plastic deformation found in the fracture specimen of PZn2, suggesting fewer interlocking sites and support for the poor bonding with the lacquer. On a microscale, interstices of 5–15 μm in size 1–2 μm deep and uniformly distributed, characterize the PZn1 surface, while smaller (< 1 μm), fewer and superficial (< 0.1 μm) interstices are typically observed on the PZn2 surface. The interstices contribute to the mechanical force component of the adhesion by supplying locations for the lacquer molecules constituting the film to penetrate into the phosphate film and to provide mechanical fastening of the film to the surface [3, 8]. Cross-sectional studies would be useful in establishing whether interpenetration of coating into the phosphating film does occur, and, if so, at what level, and to define the geometry and mechanisms of the toughening mode.

The influence of increasing the stoving temperature in the case of an SPZn2L system resulted in lower USS_{net} values rather than in an increase. This result is contrary to that found with SPZn1L and SL systems in this work, or with the SPL system in a previous study. We assume that at a higher stoving temperature (220 °C) stronger bonds at the polymer–PZn2 interface region are created due to an increased degree of polymer crosslinking. These stronger bonds obviously induced an easier failure, at lower stress, along the discontinuous plane of least cohesion within the unusual layered structure of PZn2 material. Intrinsic stresses within the relatively thick (~ 2.4 μm) PZn2 film, as introduced by the increase in stoving temperature – e.g. structural changes – could also contribute to weakening the adhesion bonds.

There is little practical evidence that adhesion of coatings to thicker films is superior to that on thinner films. Sugama *et al.* [9] have shown that adhesion strength decreases with increasing zinc phosphate thickness. Previous results with iron-phosphated cold-rolled steel [16] have shown the appearance of microcracks in thicker films. Crack generation in the PZn2 samples could also occur due to the tensile stress in the coatings when it reaches a certain thickness which coincides with the release of internal stresses. These cracks, which act as stress raisers, may also trigger the failure due to high stress concentration. The moderate increase in USS_{net} value in the case of the SPZn1L system with an increase in stoving temperature in the range of 200–220 °C suggests that some structural change within the PZn1 layer occurred as well, which probably altered the wholeness of the layer. Previous TEM studies [16] with iron phosphate have shown that heating at temperatures > 200 °C for 15 min induced occasional microcracks in the film which might be related to the difference in the thermal expansion between the layers and the substrate, and to coarsening of particles and preferred orientation.

6. Conclusions

In this study we applied a shear test to quantify the relative toughness of the bond of a fast-cure thermosetting powder coating to zinc phosphated cold-rolled steel.

Results have shown that zinc phosphating promotes adhesion by changing the interface chemistry and surface microtopography of the cold-rolled steel base material having no bulk chemical affinities with the lacquer, provided that its own integrity has not been weakened in the process.

Acknowledgements

This research was supported by a grant from the Chief Scientist of the Israel Ministry of Commerce and Industry. We wish to thank Mrs Lelia Arcan (ARO) for SEM facilities, Professor M. Arcan (Tel Aviv University) for helpful discussions and Mr O. Rabina and Mrs Mazal Bery (Pachmas) for producing the samples. Y. M. Aravot thanks the Levy Eshkol Fund for a PhD student scholarship.

References

1. T. SUGAMA, L. E. KUKACKA, N. CARCIELLO and J. B. WARREN, *J. Mater. Sci.* **22** (1987) 722.
2. W. J. van OOIJ and T. H. VISSER, *Spectrochim. Acta* **39B** (1984) 1541.

3. T. SUGAMA, L. E. KUKACKA, N. CARCIELLO and J. B. WARREN, *J. Mater. Sci.* **23** (1988) 101.
4. W. FUNKE, in ACS Symposium Series 322 (1986) edited by Dickie and Floyd, p. 222.
5. A. J. KINLOCH, in "Adhesion and Adhesives" (Chapman and Hall, London, 1987) p. 57.
6. *Idem, J. Mater. Sci.* **15** (1980) 2141.
7. N. SATO, *Surf. Coat. Technol.* **30** (1987) 171.
8. D. L. TRAWINSKI, D. K. McNAMARA and J. D. VENABLES, *SAMPE Quart.* **6** (1984) 6.
9. T. SUGAMA, L. E. KUKACKA, N. CARCIELLO and J. B. WARREN, *J. Appl. Polym. Sci.* **30** (1985) 2137.
10. L. ARCAN, M. ARCAN, Y. M. ARAVOT, O. RABINA and A. ALBU-YARON, *Ultramicroscopy* **23** (1987) 234.
11. Y. M. ARAVOT, L. ARCAN, M. ARCAN and A. ALBU-YARON, *J. Mater. Sci.* **25** (1990) 3714.
12. M. ARCAN, Z. HASHIN and A. VOLOSHIN, *Exp. Mech.* **18** (1978) 141.
13. A. N. GENT, *Rubber Chem. Technol.* **47** (1974) 202.
14. V. WEISSBERG and M. ARCAN, in "Experimental Stress Analysis", edited by M. Wieringa (Nijhoff, Amsterdam, 1986) p. 255.
15. R. J. GOOD, ASTM STP 640 (American Society for Testing and Materials, Philadelphia, 1978) p. 14.
16. A. ALBU-YARON and O. RABINA, *Thin Solid Films* **162** (1988) 183.

Received 23 July 1990
and accepted 6 February 1991